Characterization of the CYP2C8 Active Site by Homology Modeling

Toshimasa TANAKA,* Naomi KAMIGUCHI, Teruaki OKUDA, and Yoshio YAMAMOTO

Pharmaceutical Research Division, Takeda Chemical Industries, Ltd.; 2–17–85 Juso-Honmachi, Yodogawa-ku, Osaka 532–8686, Japan. Received March 8, 2004; accepted April 14, 2004; published online April 19, 2004

To compare the features of the active sites of CYP2C8, CYP2C9, and CYP2C19, homology modeling was performed based on the crystallographic coordinates of mammalian CYP2C5. It was found that CYP2C8 has a much larger pocket than the other forms due to the existence of an additional pocket. The approach to the additional pocket is comprised of Ile102, Ser114, Leu208, Val366, and Ile476, and the side chains of Ser114, Val366, and Ile476, which are smaller than the corresponding residues in the other CYPs, enable access to the pocket. The general features of the active site in the CYP2C8 model are similar to those of the previously constructed CYP3A4 model, which may account for the 2 CYPs sharing some of their substrates. The CYP2C8 model was validated by examining the bound orientation of paclitaxel and showing that it is consistent with the formation of the 6-beta hydroxylated derivative during metabolism. Docked paclitaxel was found to form a hydrogen bond with the side chain of Asn 99, which is a characteristic residue of CYP2C8 and is located in the additional pocket. Descriptors for CYP2C8 and CYP2C9 substrates were also examined with the molecular operating environment (MOE). The descriptor by which CYP2C8 and CYP2C9 substrates were classified most distinctly was found to be molar refractivity, which might be related to the longer shape and more polar nature of the active site of CYP2C8 in the CYP2C subfamily.

Key words CYP2C8; CYP3A4; homology modeling; docking model; drug–drug interaction; cytochrome P450

Cytochrome P450s (CYPs) are membrane-associated heme proteins and hepatic microsomal enzymes participating in drug metabolism and detoxification. Among the human CYPs, CYP3A4 is the most important enzyme because of its participation in a wide range of drug metabolism and high level of expression in the human liver.[1,2] On the other hand, in the CYP2C subfamily, CYP2C9 (*e.g.* fluoxetine, losartan, phenytoin, tolbutamide, torsemide, S-warfarin, and NSAIDs[3]) and CYP2C19 (*e.g.* antidepressants, proton pump inhibitors, benzodiazepines, S-mephenytoin, and proguanil[4—6]) are known to catalyze reactions for a lot of therapeutic agents. However, recently it has become clear that the contribution of CYP2C8 to drug metabolism has been underestimated, and CYP2C8 and CYP3A4 share some of their substrates (*e.g.* repaglinide, paclitaxel, morphine, carbamazepine, verapamil, zopiclone, and cerivastatin.[7—13]).

The crystal structure of mammalian CYP2C5 reported by Williams *et al.*[14] has enabled modeling of human CYPs. Thus, we have constructed CYP2C8, CYP2C9, and CYP2C19 models based on the CYP2C5 crystallographic coordinates, and compared them with the previously constructed CYP3A4 model[15] to elucidate the differences in their active sites. These models could be used to obtain helpful hints for avoiding undesirable drug–drug interactions.

Experimental

Homology Modeling The amino acid sequences of CYP2C8, CYP2C9, and CYP2C19 were taken from the ExPASy web site (http://tw.expasy.org/). The amino acid sequence alignment used for the homology modeling was obtained by ClustalW.[16] According to the alignment (Fig. 1), homology models of CYP2C8, CYP2C9, and CYP2C19 were constructed based on the mammalian CYP2C5 crystal structure (PDB code:1DT6) using the homology module of Insight II (ver. 2000, Accelrys Inc., San Diego, California, U.S.A.). Using the Search/Generate-Loops function of Insight II, conformations of the insertion parts in the alignment were generated. After some manual adjustments to remove large steric hindrances, the whole structure was subjected to energy minimization over 1000 steps with the steepest descent minimizer and then 5000 steps with the conjugate gradient minimizer, to a maximum gradient of 0.1 kcal/mol^{-1} Å^{-1}, using the Discover-ESFF force field (ver. 980, Accelrys Inc., San Diego, California, U.S.A.). During the minimization procedure, the following conditions were adopted. The dielectric constant was set to 4*r, where r is the distance between two interacting atoms. The force constant of tethering constraints for the backbone of structurally conserved regions (SCRs, asterisks in Fig. 1) and heme was set to 40 kcal/Å^2 to prevent a large movement from the initial positions.

Docking of Paclitaxel Paclitaxel, an anticancer drug from a natural compound, was docked into the CYP2C8 model using Gold (ver. 2.0, the

Fig. 1. Alignment of Amino Acid Sequences among CYP2C5, CYP2C8, CYP2C9, CYP2C19, and CYP3A4

Alpha-helices and beta-sheets are shown by double and single underlines, respectively. Asterisks indicate structurally conserved regions (SCRs) among the known 3-D structures.

* To whom correspondence should be addressed. e-mail: Tanaka_Toshimasa@takeda.co.jp

Cambridge crystallographic data centre, U.K.[17]) with the standard default settings. Among the 10 binding modes obtained, the best scored orientation was subjected to energy minimization with the enzyme, using the Discover-ESFF force field. The condition of the minimization procedure is the same as that described in the homology modeling section.

Pharmacophore Search and Docking of CYP2C8 Substrates The pharmacophore for 7 substrates (17beta-estradiol, fluvastatin acid, omeprazole, rosiglitazone, seratrodast, tienilic acid, and paclitaxel, Fig. 5b) that are hydroxylated by CYP2C8, was explored with Catalyst HipHop (ver. 4.7, Accelrys Inc., San Diego, California, U.S.A.). Eight metabolite surrogates (2 for 17beta-estradiol and 1 for the others), in which an aminomethyl group was introduced at the hydroxylated position of each of the 7 substrates, were used in the HipHop calculation. The minimum number of cationic ionizable features was set to one, to ensure the correspondence of each amino group. During the Catalyst calculation, paclitaxel was fixed to the structure in the docking model, and conformations of the other substrates were generated, up to a maximum of 250, using the 'best quality' settings of the program with an energy range of 20 kcal/mol. Ten hypotheses were generated and a hypothesis was selected on the basis of the overlap volume of all the structures. Using the superposition of the 7 metabolite surrogates on paclitaxel and the CYP2C8/paclitaxel model obtained by Gold, the initial structures of the substrate-complexed CYP2C8 models were constructed, which were then energy-minimized using the Discover-ESFF force field to obtain the final docking models.

Analysis of Chemical Properties of Substrates Chemical properties were analyzed by 2D and i3D (internal coordinate dependent 3D) descriptor calculations with MOE (ver. 2003.02, Chemical Computing Group: Montreal, Canada) for arbitrarily selected CYP2C8 and CYP2C9 substrates from the literature. The selected 48 substrates of CYP2C8 are antipyrine, diclofenac, ibuprofen, methadone, naproxen, dapsone, trimethoprim, mitrazapine, rosiglitazone, tolbutamide, troglitazone, carbamazepine, phenytoin, trimethadione, terbinafine, halofantrine, ifosfamide, paclitaxel, tegafur, clozapine, zidovudine, diazepam, temazepam, zopiclone, amiodarone, bufuralol, diltiazem, gallopamil, nicardipine, norverapamil, seratrodast, tienilic acid, torasemide, verapamil, warfarin, cisapride, lansoprazole, omeprazole, propofol, cerivastatin, fluvastatin, lidocaine, retinol, benzo[a]pyrene, methoxychlor, arachidonic acid, 17beta-estradiol, and tetrahydrocannabinol,[18]) and the selected 75 substrates of CYP2C9 are aceclofenac, aspirin, diclofenac, ibuprofen, indomethacin, lornoxicam, antipyrine, celecoxib, flurbiprofen, meloxicam, methadone, naproxen, piroxicam, suprofen, tenoxicam, dapsone, trimethoprim, amitriptyline, deprenyl, mirtazapine, moclobemide, sertraline, venlafaxine, rosiglitazone, tolbutamide, troglitazone, phenobarbital, phenytoin, trimethadione, terbinafine, cinnarizine, flunarizine, proguanil, tolterodine, ifosfamide, tamoxifen, tauromustine, clozapine, perphenazine, amprenavir, zidovudine, diazepam, flunitrazepam, temazepam, zolpidem, zopiclone, zafirlukast, candesartan, carvedilol, diltiazem, dorzolamide, irbesartan, losartan, seratrodast, tienilic acid, torasemide, verapamil, warfarin, dextromethorphan, retinoic acid, sildenafil, dolasetron, lansoprazole, omeprazole, ondansetron, tropisetron, zileuton, propofol, fluvastatin, lidocaine, benzo[a]pyrene, methoxychlor, arachidonic acid, desogestrel, and 17beta-estradiol.[18])

The descriptor by which CYP2C8 and CYP2C9 substrates are classified most distinctly was determined by the QuaSAR-Classify function of MOE with the cross-validation protocol among the 2D and i3D descriptors.

Results and Discussion

The pocket of the CYP2C8 model is much larger (740 Å^3) than the pockets of the CYP2C5 crystal structure (420 Å^3), the CYP2C9 model (510 Å^3), and the CYP2C19 model (510 Å^3). The larger pocket of CYP2C8 might be attributed to the existence of an additional pocket (the distal site 2 in Fig. 2a). In the CYP2C8 model, the approach to the additional pocket is comprised of Ile102, Ser114, Leu208, Val366, and Ile476 (Fig. 2b), and the side chains of Ser114, Val366, and Ile476, which are smaller than the corresponding residues in the other CYPs, enable access to this pocket. On the other hand, larger amino acids of CYP2C5 (Phe114, Leu363, and Phe473), CYP2C9 (Phe114, Leu366, and Phe476), and CYP2C19 (Phe114, Leu366, and Phe476) at the corresponding positions occlude the access (Figs. 2d—f). The corresponding residues in the previously constructed CYP3A4 model[15]) are Pro110, Ile120, Asp214, Leu373, and Leu479 (Fig. 2c), which also enable access to the additional pocket and contribute partly to its large active site (950 Å^3). Thus the active site of CYP2C8 is estimated to be similar to that of CYP3A4 in terms of volume and shape, and the resemblance of the active sites may be one of the reasons that CYP2C8 and CYP3A4 share some of their substrates.

In order to clarify the differences in the active sites, the positions of dissimilar amino acids around the heme of the CYP2C models, in terms of side chain characters, were checked. There were found to be 4 main positions that differ: Asn99, Ser114, Phe205, and Ile476 of CYP2C8, Ser99, Phe114, Val205, and Phe473 of CYP2C5, Ile99, Phe114, Ile205, and Phe476 of CYP2C9, His99, Phe 114, Ile205, and Phe476 of CYP2C19 (Fig. 3). Consequently, the CYP2C8 active site might be comparatively more polar than the CYP2C5, CYP2C9, and CYP2C19 ones because of the existence of the two polar residues, Asn99 and Ser114.

It is known that paclitaxel is hydroxylated at the 6-beta position by CYP2C8.[19—21]) Using Gold, paclitaxel was found to adopt an orientation that can explain the formation of the 6-beta hydroxylated metabolite (Fig. 4a). The bulky taxane skeleton was docked into the proximal site, which is larger than that of the CYP3A4 model. In the previous study,[15]) the substituent at the C3′ position of paclitaxel was presumed to be bound to the proximal pocket of CYP3A4 (Fig. 4b). These docking models, therefore, explain the reason why CYP2C8 and CYP3A4 catalyze different positions of paclitaxel. In the CYP2C8 model, paclitaxel forms a hydrogen bond with the side chain of Asn99, which is one of the characteristic residues in CYP2C8, as discussed above.

In addition to paclitaxel, 6 substrates hydroxylated by CYP2C8 (17beta-estradiol,[22]) fluvastatin acid,[13,23,24]) omeprazole,[25,26]) rosiglitazone,[27]) seratrodast[28]) and tienilic acid,[29—31]) Fig. 5b) were docked into the CYP2C8 model with Gold. However, various orientations were presented for each substrate, and they did not necessarily contain a binding mode consistent with the formation of the metabolites. Therefore we applied a pharmacophore search of Catalyst-HipHop to the substrates to determine the initial structures of the substrate-complexed models. During the HipHop calculation, the structure of each substrate was modified by substitution of an aminomethyl group at the hydroxylated position. In these modifications, we considered the nitrogen atoms in the aminomethyl substituents as surrogates for the heme iron. The aminomethyl group can be treated as a sole cationic ionizable feature in the calculation to ensure reasonable superposition, because all selected substrates have no aliphatic amino group. The pharmacophore hypothesis, in which the metabolite surrogates were superposed with the largest intersection volumes, contains a hydrophobic area, a hydrogen bond acceptor, and a cationic ionizable group (Fig. 5a). In the 7 docking models of the 6 substrates (17beta-estradiol is hydroxylated at two positions), constructed on the basis of superposition on the paclitaxel surrogate, all the substrates fit in the pocket (Fig. 6).

Finally, when the descriptors for CYP2C8 and CYP2C9 substrates were examined with MOE, contrary to our expectation, there was little difference between the two regarding their molecular weight, molecular volume, water accessible

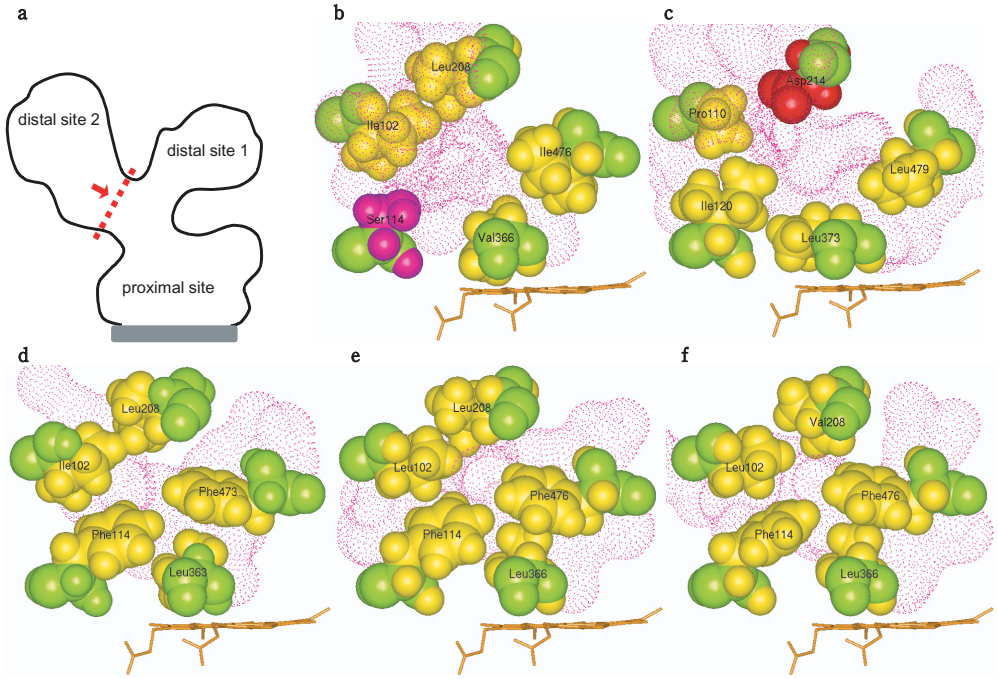

Fig. 2. Comparison of Amino Acids at the Approach to the Putative Additional Pocket (Distal Site 2)

Red dotted line in (a) (the diagram sketch of the putative active site) indicates the approach to the additional pocket. CPK representations of the amino acids at the approach to the additional pocket (distal site 2) in (b) the CYP2C8 model, (c) the CYP3A4 model, (d) the CYP2C5 crystal structure, (e) the CYP2C9 model, and (f) the CYP2C19 model.

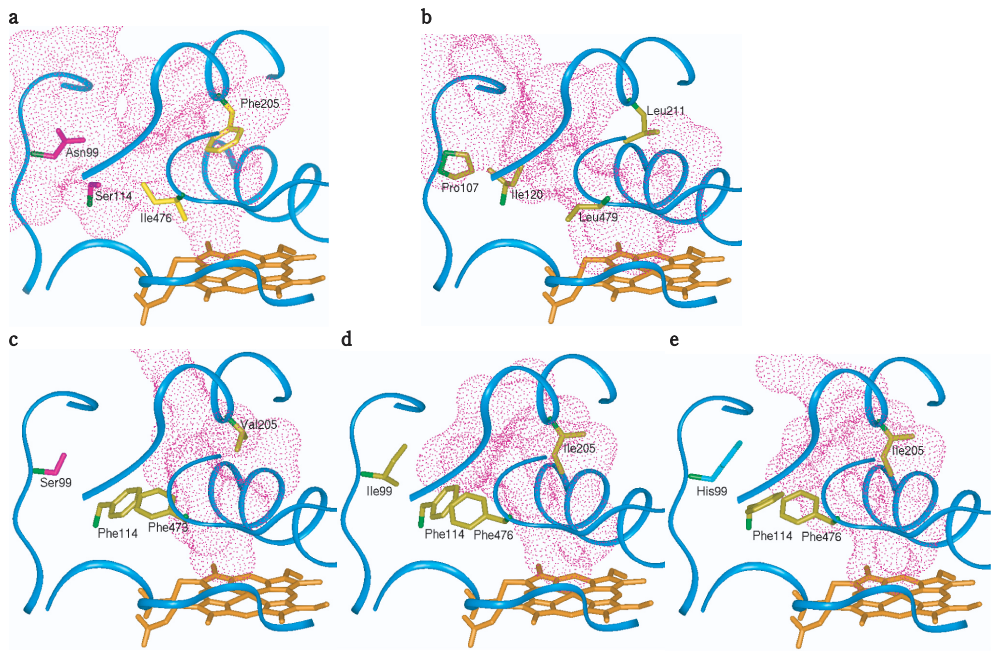

Fig. 3. Comparison of Dissimilar Amino Acids in the Active Sites

Characteristic 4 residues in (a) the CYP2C8 model, (b) the CYP3A4 model, (c) the CYP2C5 crystal structure, (d) the CYP2C9 model, and (e) the CYP2C19 model are shown with residue names. In each model, heme is shown in orange stick, the shape of the pocket in magenta dot surface, and the main chain in cyan ribbon.

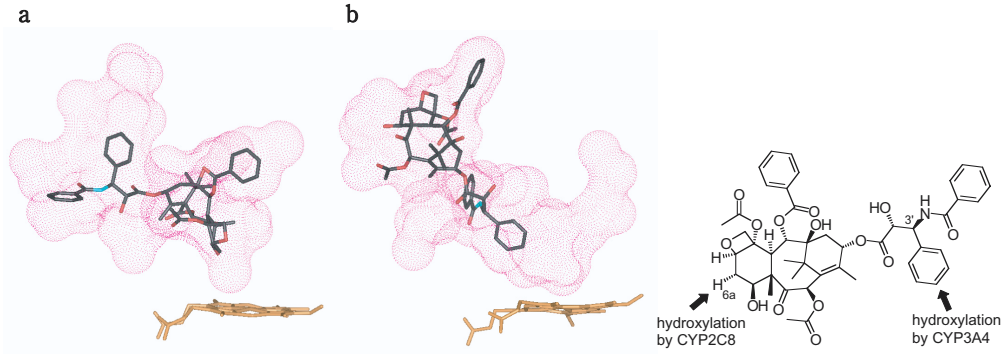

Fig. 4. Paclitaxel Docked into (a) the CYP2C8 Model and (b) the CYP3A4 Model

Paclitaxel is shown in black stick, heme in orange stick , and the shape of the pocket in magenta dot surface.

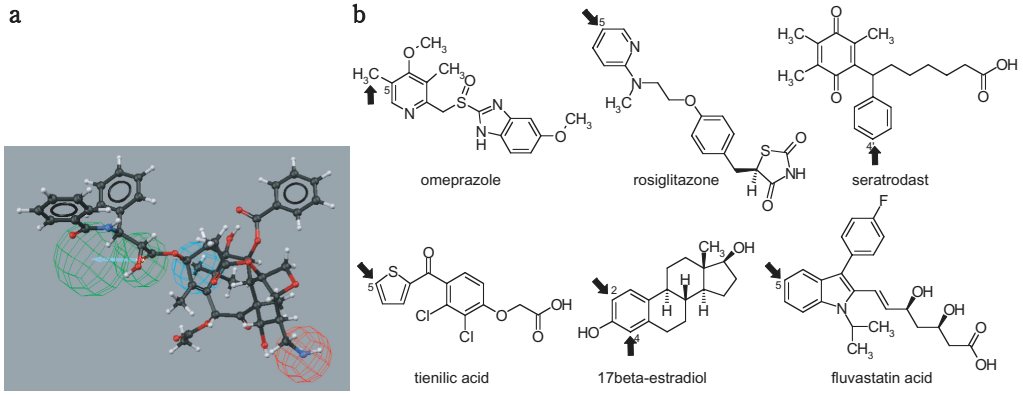

Fig. 5. (a) The Selected Pharmacophore for 6 Substrates Hydroxylated by CYP2C8

It contains a hydrogen bond acceptor (a pair of green spheres), a hydrophobic area (cyan sphere), and a cationic ionizable group (red sphere). The hydroxylated position of paclitaxel is substituted by an aminomethyl moiety as a heme iron surrogate.

(b) Chemical Structures of the Used CYP2C8 Substrates

Arrows indicate the positions of hydroxylation by CYP2C8.

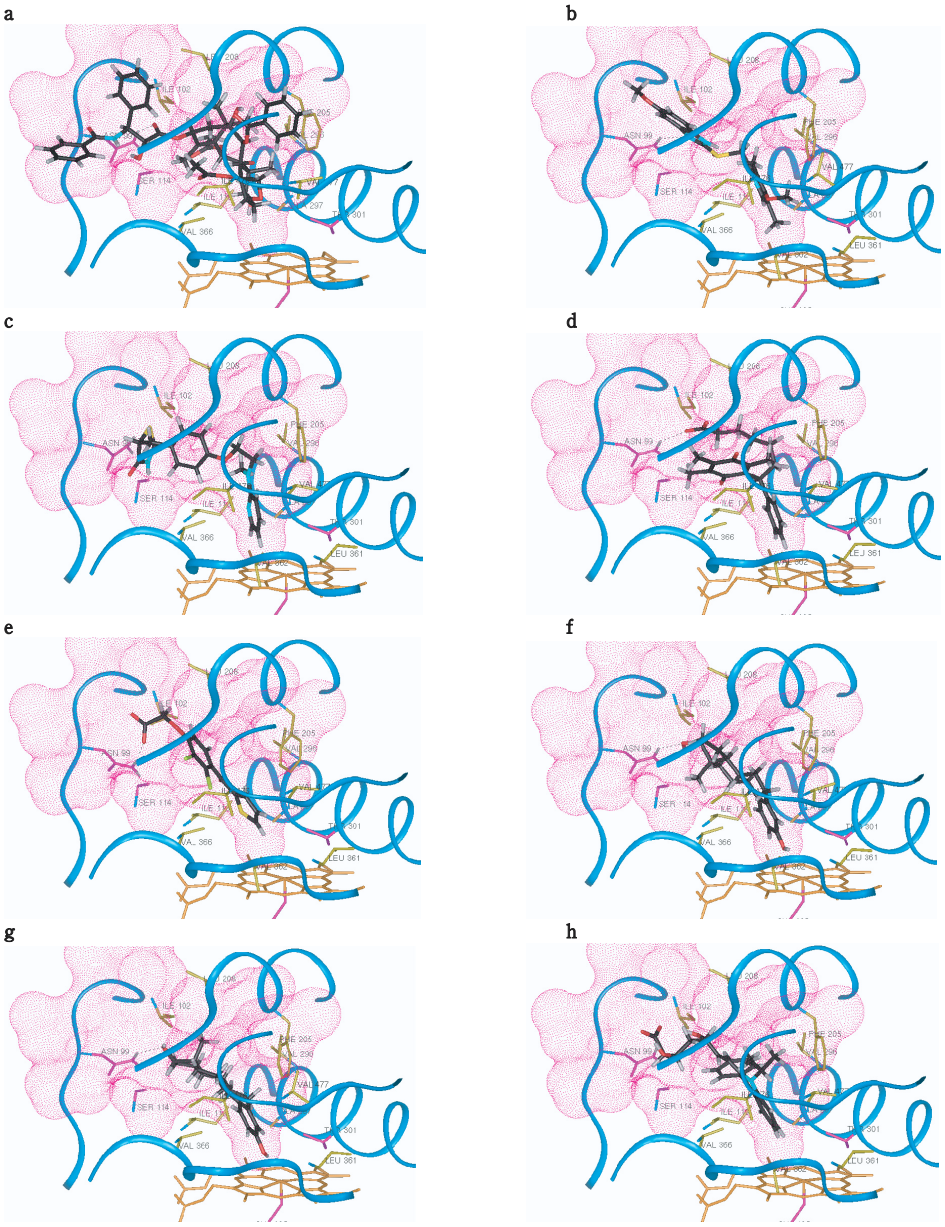

Fig. 6. Docking Models for 7 Substrates (Two Models for 17beta-Estradiol)

The bound molecules are (a) paclitaxel, (b) omeprazole, (c) rosiglitazone, (d) seratrodast, (e) tienilic acid, (f) (g) 17beta-estradiol, and (h) fluvastatin acid.

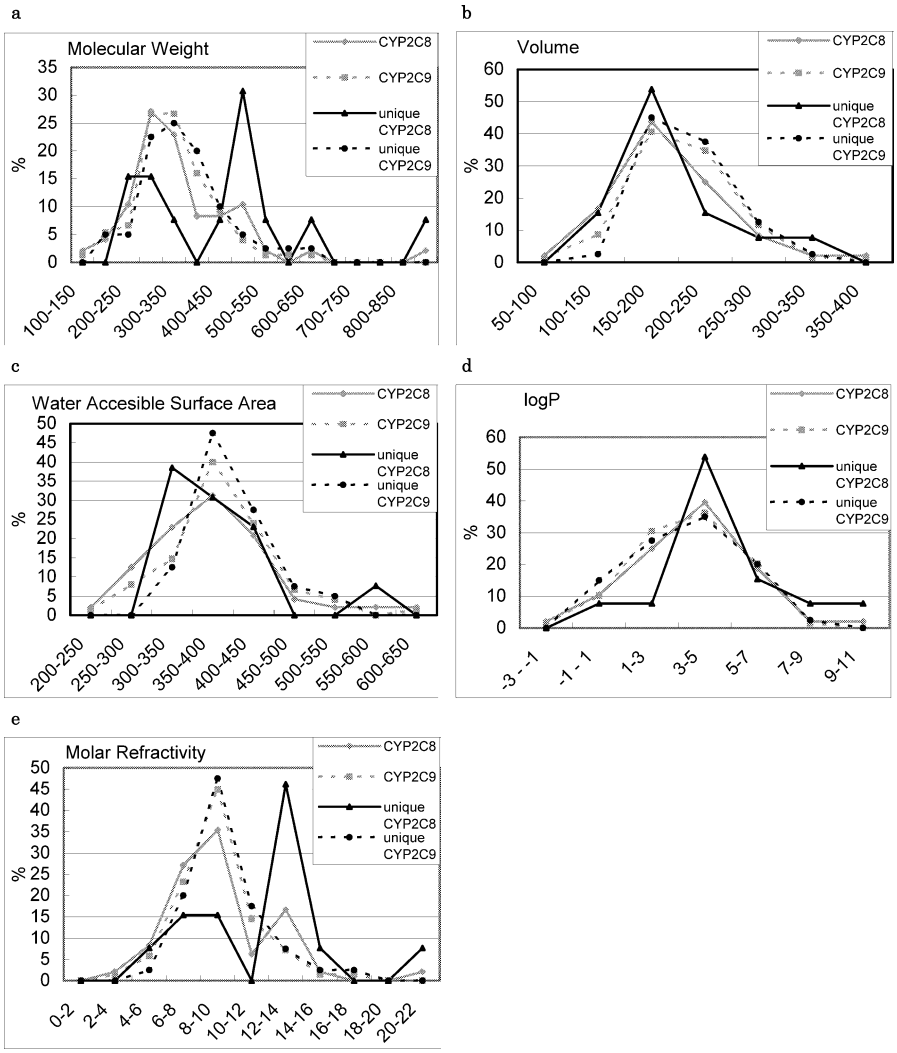

Fig. 7. Comparison of Chemical Properties for CYP2C8 and CYP2C9 Substrates

(a) Molecular weight, (b) molecular volume, (c) water accessible surface area, (d) log P, (e) molecular refractivity.

surface area (ASA), log P and molar refractivity (SMR) (gray lines in Figs. 7a—e). Since there is a possibility that dual substrates for CYP2C8 and CYP2C9 (35 compounds) may make the result unclear, we also calculated the chemical properties without them. While molecular weight (black lines in Fig. 7a) and molar refractivity (black lines in Fig. 7e) became more separated, molecular volume, ASA, and log P (black lines in Figs. 7b—d) displayed little difference. The similarity for molecular volume is the most unexpected result from the exploration of homology modeling because the active site volumes differ a great deal. The difference for molar refractivity, which represents size and polarizability of a molecule,[32] might be related to the longer shape and more polar nature of the active site of CYP2C8. The latter feature may be due to the existence of polar residues, Asn99 and Ser114, in the additional pocket. Although the number of compounds reported as CYP2C8 substrates is currently limited, increasing information about CYP2C8 metabolism will make the analysis more accurate.

After we had explored homology modeling of the CYP2C subfamily, the crystal structures of human CYP2C9[33] and human CYP2C8[34] were reported. Our models of CYP2C9 and CYP2C8 were confirmed to be quite similar to the crystal structures, except the region between the F and G. helices.

Conclusions

We have constructed CYP2C8, CYP2C9, and CYP2C19 models, utilizing the available crystal structure of mammalian CYP2C5. It has been found that the active site of CYP2C8 is much larger and comparatively more polar than the other members of the subfamily. The larger pocket of CYP2C8 is presumed to be due to the existence of an additional pocket, which is also observed in the previously constructed CYP3A4 model. All the 7 substrates docked into the CYP2C8 model, fit in the large pocket. The descriptor of MOE by which CYP2C8 and CYP2C9 substrates were classified most distinctly was molar refractivity. The result might be related to the longer shape and more polar nature of the CYP2C8 active site.

References and Notes

1) Bertz R. J., Granneman G. R., *Clin. Pharmacokinet.*, **32**, 210—258 (1997).
2) Shimada T., Yamazaki H., Mimura M., Inui Y., Guengerich F. P., *J. Pharmacol. Exp. Ther.*, **270**, 414—423 (1994).
3) Miners J. O., Birkett D. J., *Br. J. Clin. Pharmacol.*, **45**, 525—538 (1998).

4) Bertilsson L., *Clin. Pharmacokinet.*, **29**, 192—209 (1995).
5) Coller J. K., Somogyi A. A., Bochner F., *Xenobiotica*, **29**, 973—986 (1999).
6) Xu Z. H., Wang W., Zhao X. J., Huang S. L., Zhu B., He N., Shu Y., Liu Z. Q., Zhou H. H., *Br. J. Clin. Pharmacol.*, **48**, 416—423 (1999).
7) Bidstrup T. B., Bjornsdottir I., Sidelmann U. G., Thomsen M. S., Hansen K. T., *Br. J. Clin. Pharmacol.*, **56**, 305—314 (2003).
8) Monsarrat B., Chatelut E., Royer I., Alvinerie P., Dubois J., Dezeuse A., Roché H., Cros S., Wright M., Canal P., *Drug Metab. Dispos.*, **26**, 229—233 (1998).
9) Projean D., Morin P. E., Tu T. M., Ducharme J., *Xenobiotica*, **33**, 841—854 (2003).
10) Kerr B. M., Thummel K. E., Wurden C. J., Klein S. M., Kroetz D. L., Gonzalez F. J., Levy R. H., *Biochem. Pharmacol.*, **47**, 1969—1979 (1994).
11) Tracy T. S., Korzekwa K. R., Gonzalez F. J., Wainer I. W., *Br. J. Clin. Pharmacol.*, **47**, 545—552 (1999).
12) Becquemont L., Mouajjah S., Escaffre O., Beaune P., Funck-Brentano C., Jaillon P., *Drug Metab. Dispos.*, **27**, 1068—1073 (1999).
13) Prueksaritanont T., Ma B., Tang C., Meng Y., Assang C., Lu P., Reider P. J., Lin J. H., Baillie T. A., *Br. J. Clin. Pharmacol.*, **47**, 291—298, (1999).
14) Williams P. A., Cosme J., Sridhar V., Johnson E. F., McRee D. E., *Mol. Cell*, **5**, 121—131 (2000).
15) Tanaka T., Okuda T., Yamamoto Y., *Chem. Pharm. Bull.*, **52**, 830—835 (2004).
16) Thompson J. D., Higgins D. G., Gibson T. J., *Nucleic Acids Res.*, **22**, 4673—4680 (1994).
17) Jones G., Willett P., Glen R. C., Leach A. R., Taylor R., *J. Mol. Biol.*, **267**, 727—748 (1997).
18) Rendic S., *Drug Metab. Rev.*, **34**, 83—448 (2002).
19) Cresteil T., Monsarrat B., Alvinerie P., Treluyer J. M., Vieira I., Wright M., *Cancer Res.*, **54**, 386—392 (1994).
20) Rahman A., Korzekwa K. R., Grogan J., Gonzalez F. J., Harris J. W., *Cancer Res.*, **54**, 5543—5546 (1994).
21) Cresteil T., Monsarrat B., Dubois J., Sonnier M., Alvinerie P., Gueritte F., *Drug Metab. Dispos.*, **30**, 438—445 (2002).
22) Satoh T., Fujita K. I., Munakata H., Itoh S., Nakamura K., Kamataki T., Itoh S., Yoshizawa I., *Anal. Biochem.*, **286**, 179—186 (2000).
23) Fischer V., Johanson L., Heitz F., Tullman R., Graham E., Baldeck J. P., Robinson W. T., *Drug Metab. Dispos.*, **27**, 410—416 (1999).
24) Scripture C. D., Pieper J. A., *Clin. Pharmacokinet.*, **40**, 263—281 (2001).
25) Karam W. G., Goldstein J. A., Lasker J. M., Ghanayem B. I., *Drug Metab. Dispos.*, **24**, 1081—1087 (1996).
26) Ibeanu G. C., Ghanayem B. I., Linko P., Li L., Pederson L. G., Goldstein J. A., *J. Biol. Chem.*, **271**, 12496—12501, (1996).
27) Baldwin S. J, Clarke S. E., Chenery R. J., *Br. J. Clin. Pharmacol.*, **48**, 424—432 (1999).
28) Kumar G. N., Dubberke E., Rodrigues A. D., Roberts E., Dennisen J. F., *Drug Metab. Dispos.*, **25**, 110—115 (1997).
29) Spatzenegger M., Jaeger W., *Drug Metab. Rev.*, **27**, 397—417 (1995).
30) Slaughter R. L., Edwards D. J., *Pharmacokinetics*, **29**, 619—624 (1995).
31) Jean P., Lopez-Garcia P., Dansette P., Mansuy D., Goldstein J. L., *Eur. J. Biochem.*, **241**, 797—804 (1996).
32) Wildman S. A., Crippen G. M., *J. Chem. Inf. Comput. Sci.*, **39**, 868—873 (1999).
33) Williams P. A., Cosme J., Ward A., Angove H. C., Matak Vinkovic D., Jhoti H., *Nature* (London), **424**, 463—468 (2003).
34) Schoch G. A., Yano J. K., Wester M. R., Griffin K. J., Stout C. D., Johnson E. F., *J. Biol. Chem.*, **279**, 9497—9503, (2004).